 CMES, vol.22, no.2, pp.151-164, 2007

# Boundary Element Analysis of Three-Dimensional Exponentially Graded Isotropic Elastic Solids

**R. Criado[1], J.E. Ortiz[1], V. Mantič[1], L.J. Gray[1,2] and F. París[1]**

**Abstract:** A numerical implementation of the Somigliana identity in displacements for the solution of 3D elastic problems in exponentially graded isotropic solids is presented. An expression for the fundamental solution in displacements, $U_{j\ell}$, was deduced by Martin et al. (*Proc. R. Soc. Lond. A*, **458**, pp. 1931–1947, 2002). This expression was recently corrected and implemented in a Galerkin indirect 3D BEM code by Criado et al. (*Int. J. Numer. Meth. Engng.*, 2008). Starting from this expression of $U_{j\ell}$, a new expression for the fundamental solution in tractions $T_{j\ell}$ has been deduced in the present work. These quite complex expressions of the integral kernels $U_{j\ell}$ and $T_{j\ell}$ have been implemented in a collocational direct 3D BEM code. The numerical results obtained for 3D problems with known analytic solutions verify that the new expression for $T_{j\ell}$ is correct. Excellent accuracy is obtained with very coarse boundary element meshes, even for a relatively high grading of elastic properties considered.

**Keyword:** functionally graded materials, boundary element method, three-dimensional elasticity, Somigliana identity, fundamental solution in tractions.

## 1 Introduction

Functionally Graded Materials (FGMs) [Suresh and Mortensen (1998)] represent a new generation of composites, having a continuous variation of apparent material properties obtained through a progressive variation of their microstructural composition. Stress concentrations appearing at material discontinuities in various applications (for example, thermal barrier coatings) can be avoided or diminished using FGMs.

The first numerical studies of FGMs have been carried out using the Finite Element Method (FEM) [Lee and Erdogan (1998); Santare and Lambros (2000); Anlas *et al.* (2000); Kim and Paulino (2002a,b); Paulino and Kim (2004)] due to its capability to include, relatively easily, variation of material properties. The Meshless Local Petrov-Galerkin (MLPG) Method [Atluri and Shen (2002); Sládek *et al.* (2004, 2005, 2007); Ching and Chen (2006)] has also recently shown to be a versatile approach to solve different problems including non-homogeneous media.

The Boundary Element Method (BEM) [París and Cañas (1997); Aliabadi (2002)] is another technique for elastic analysis, capable of solving problems with material and geometrical discontinuities, *e.g.*, crack growth and contact, and also very suitable for flaw detection and shape optimization. Nevertheless, an adaption of BEM to non-homogeneous media is a hard task, as fundamental solutions or Green's functions (corresponding to concentrated loads or sources) for such media are difficult to obtain.

Fundamental solutions for heat transfer problems in non-homogeneous media have been presented in Shaw and Makris (1992); Clements (1998); Gray *et al.* (2003); Berger *et al.* (2005) and Kuo and Chen (2005) and implemented in BEM codes by Gray *et al.* (2003); Clements and Budhi (1999); Núñez *et al.* (2002); Paulino *et al.* (2002) and Sutradhar and Paulino (2004). Green's functions due to surface loads in non-homogeneous half-spaces have been deduced in Han *et al.* (2006) and Seyrafian *et al.* (2006).

Fundamental solutions for 2D and 3D elastic

[1] School of Engineering, University of Seville, Camino de los Descubrimientos s/n, Sevilla, E-41092, Spain

[2] Computer Science and Mathematics Division, Oak Ridge National Laboratory, Oak Ridge, TN 37831-6367, USA

problems in exponentially graded isotropic materials have been deduced only recently in Chan *et al.* (2004) and Martin *et al.* (2002). These solutions have not as yet been checked computationally, to the knowledge of the present authors, which can be due to the fact that implementing them in a BEM code is far from straightforward.

In the present work the displacement fundamental solution $U_{jl}$ corresponding to a point force in a 3D exponentially graded elastic isotropic media, developed originally in Martin *et al.* (2002) and corrected by Criado and co-workers (2005, 2008), is employed in the form presented in Criado and co-workers (2005, 2008). Moreover, a new expression of the corresponding traction fundamental solution $T_{jl}$ is presented herein, and both functions have been implemented in a 3D collocational BEM code. To check the correctness of the kernel function expressions and to prove their suitability to be implemented in a BEM code, and also to check the overall BEM implementation, two 3D problems with known analytic solutions for exponentially graded materials have been analysed by this BEM code.

## 2 Properties of Elastic Exponentially Graded Isotropic Materials

The fourth rank tensor of elastic stiffnesses $c_{ijk\ell}$ $(i,j,k,\ell = 1,2,3)$ for an exponentially graded material varies according to the following law:

$$c_{ijk\ell}(\boldsymbol{x}) = C_{ijk\ell}\exp(2\boldsymbol{\beta}\cdot\boldsymbol{x}), \tag{1}$$

where $\boldsymbol{x}$ is a point in the material and the vector $\boldsymbol{\beta}$ defines the direction and exponential variation of grading, $\beta = \|\boldsymbol{\beta}\|$. According to (1), points situated in a plane perpendicular to $\boldsymbol{\beta}$ have the same stiffnesses, $C_{ijk\ell}$ giving the stiffnesses in the plane including the origin of coordinates.

In the case of isotropic materials, the Lamé constants $\lambda$ and $\mu$ satisfy

$$c_{ijk\ell}(\boldsymbol{x}) = \lambda(\boldsymbol{x})\delta_{ij}\delta_{k\ell} + \mu(\boldsymbol{x})\left(\delta_{ik}\delta_{j\ell} + \delta_{i\ell}\delta_{jk}\right), \tag{2}$$

where $\delta_{ij}$ is Kronecker delta, and hence for exponential grading

$$\begin{aligned} &\lambda(\boldsymbol{x}) = \lambda_0\exp(2\boldsymbol{\beta}\cdot\boldsymbol{x}) \quad \text{and} \\ &\mu(\boldsymbol{x}) = \mu_0\exp(2\boldsymbol{\beta}\cdot\boldsymbol{x}). \end{aligned} \tag{3}$$

Here $\lambda_0$ and $\mu_0$ are the Lamé constants on the plane that includes the origin of coordinates. It is easy to check, that $\lambda(\boldsymbol{x})/\mu(\boldsymbol{x}) = \lambda_0/\mu_0 = 2\nu/(1-2\nu)$, $\nu$ being the (constant) Poisson ratio defined as $\nu = \lambda_0/2(\lambda_0+\mu_0)$. Note that the assumption of a constant Poisson ratio appears to be reasonable for many real graded materials, and is a commonly used approximation in an analysis of graded materials.

## 3 Elastic Fundamental Solution in 3D Exponentially Graded Isotropic Materials

### 3.1 Displacement fundamental solution

According to Martin *et al.* (2002), the displacement fundamental solution can be written as

$$\begin{aligned} \mathbf{U}(\boldsymbol{x},\boldsymbol{x}') = &\exp\{-\boldsymbol{\beta}\cdot(\boldsymbol{x}+\boldsymbol{x}')\} \\ &\cdot\left\{\mathbf{U}^0(\boldsymbol{x}-\boldsymbol{x}') + \mathbf{U}^g(\boldsymbol{x}-\boldsymbol{x}')\right\}, \end{aligned} \tag{4}$$

where $U_{j\ell}(\boldsymbol{x},\boldsymbol{x}')$ gives the $j$-th displacement component at $\boldsymbol{x}$ due to a unit point force acting in the $\ell$-direction at point $\boldsymbol{x}'$, and $\mathbf{U}^0$ is the weakly singular Kelvin fundamental solution associated to a homogenous isotropic material defined by $\lambda_0$ and $\mu_0$ (see París and Cañas (1997); Aliabadi (2002)). The so-called grading term

$$\begin{aligned} U^g_{j\ell}(\boldsymbol{x}-\boldsymbol{x}') = &-\frac{1}{4\pi\mu_0 r}\left(1-\mathrm{e}^{-\beta r}\right)\delta_{j\ell} \\ &+A_{j\ell}(\boldsymbol{x}-\boldsymbol{x}') \end{aligned} \tag{5}$$

is bounded for $r\to 0$ and vanishes for $\beta = 0$, $r = \|\mathbf{r}\|$ where $\mathbf{r} = \boldsymbol{x}-\boldsymbol{x}'$.

Let an orthogonal system of coordinates $(\tilde{x}_1,\tilde{x}_2,\tilde{x}_3)$, whose origin is placed at $\boldsymbol{x}'$, be defined by the orthonormal right-handed triad $\{\boldsymbol{n},\boldsymbol{m},\hat{\boldsymbol{\beta}}\}$, where $\hat{\boldsymbol{\beta}} = (\hat{\beta}_1,\hat{\beta}_2,\hat{\beta}_3) = \boldsymbol{\beta}/\beta$, and $\boldsymbol{n}$ and $\boldsymbol{m}$ are orthonormal vectors in the plane perpendicular to $\boldsymbol{\beta}$. Let the following spherical coordinate system $(r,\Theta,\Phi)$ be associated to this

coordinate system:

$$\begin{aligned} \boldsymbol{r}\cdot\boldsymbol{n} &= r\sin\Theta\cos\Phi,\\ \boldsymbol{r}\cdot\boldsymbol{m} &= r\sin\Theta\sin\Phi\\ \boldsymbol{r}\cdot\hat{\boldsymbol{\beta}} &= r\cos\Theta, \end{aligned} \tag{6}$$

where $0\le\Theta\le\pi$ and $0\le\Phi\le 2\pi$.

According to Criado and co-workers (2005, 2008) the term $A_{jl}$ is composed of the following five integrals:

$$A_{jl} = -\frac{\beta}{4\pi(1-\nu)\mu_0}\mathscr{I}_1 - \frac{\beta}{2\pi^2(1-\nu)\mu_0}(\mathscr{I}_2-\mathscr{I}_3+\mathscr{I}_4-\mathscr{I}_5,), \tag{7}$$

where

$$\mathscr{I}_1 = \sum_{s=0}^{2}\sum_{n=0}^{2}\int_0^{\pi/2}\mathscr{R}_s^{(n)}\,\mathrm{e}^{-|k|y_s}\,I_n(Ky_s)\,\sin\theta\,\mathrm{d}\theta, \tag{8}$$

$$\mathscr{I}_2 = \sum_{s=0}^{2}\int_{\theta_m}^{\pi/2}\mathscr{R}_s^{(0)}\,\sin\theta\int_{\eta_m}^{\pi/2}\sinh\Psi_s\,\mathrm{d}\eta\,\mathrm{d}\theta, \tag{9}$$

$$\mathscr{I}_3 = \sum_{s=0}^{2}\int_{\theta_m}^{\pi/2}\mathscr{R}_s^{(2)}\,\sin\theta\int_{\eta_m}^{\pi/2}\sinh\Psi_s\,\cos 2\eta\cdot\mathrm{d}\eta\,\mathrm{d}\theta, \tag{10}$$

$$\mathscr{I}_4 = \sum_{s=1}^{2}\int_{\theta_m}^{\pi/2}\mathscr{M}_s^{(1)}\,\sin\theta\int_{\eta_m}^{\pi/2}\cosh\Psi_s\,\sin\eta\cdot\mathrm{d}\eta\,\mathrm{d}\theta, \tag{11}$$

$$\mathscr{I}_5 = \sum_{s=1}^{2}\int_{\theta_m}^{\pi/2}\tilde{\mathscr{M}}_s^{(1)}\,\mathrm{sgn}(k)\,\sin\theta\int_{\eta_m}^{\pi/2}\sinh\Psi_s\cdot\sin\eta\,\mathrm{d}\eta\,\mathrm{d}\theta, \tag{12}$$

the extensive notation introduced in this equation being now defined.

First, $I_n(x)$ denotes the modified first kind Bessel function of order $n$,

$$I_1(Ky_s) = \frac{2}{\pi}\int_0^{\pi/2}\sinh(Ky_s\sin\eta)\,\sin\eta\,\mathrm{d}\eta, \tag{13}$$

$$I_n(Ky_s) = \frac{2}{\pi i^n}\int_0^{\pi/2}\cosh(Ky_s\sin\eta)\,\cos n\eta\,\mathrm{d}\eta, \qquad n=0,2. \tag{14}$$

The integration limits $\theta_m$ and $\eta_m$ ($0\le\theta_m,\eta_m\le\frac{\pi}{2}$) are defined by

$$\begin{aligned} \theta_m(\Theta) &= \left|\tfrac{1}{2}\pi-\Theta\right|,\\ |k(r,\Theta,\theta)| &= K(r,\Theta,\theta)\sin\eta_m(\Theta,\theta), \end{aligned} \tag{15}$$

where $k(r,\Theta,\theta)=\beta r\cos\theta\cos\Theta$ and $K(r,\Theta,\theta)=\beta r\sin\theta\sin\Theta$, and the range of $\theta$ guarantees that $\eta_m$ is well defined. The argument of the hyperbolic functions is

$$\Psi_s(r,\Theta,\theta,\eta) = K(r,\Theta,\theta)y_s(\theta)\,(\sin\eta_m(\Theta,\theta)-\sin\eta), \tag{16}$$

where the functions $y_s$ are given by

$$\begin{aligned} y_0 &= 1,\\ y_1(\theta) &= \sqrt{q(\theta)+\sqrt{q^2(\theta)-1}},\\ y_2(\theta) &= \sqrt{q(\theta)-\sqrt{q^2(\theta)-1}}, \end{aligned} \tag{17}$$

with $q(\theta)\ge 1$ defined as

$$q(\theta) = 1+\frac{2\nu}{1-\nu}\sin^2(\theta). \tag{18}$$

The functions $\mathscr{R}_s^{(n)}$ and $\mathscr{M}_s^{(n)}$ are given by

$$\mathscr{R}_s^{(0)} = \mathscr{M}_s^{(0)}, \qquad \mathscr{R}_s^{(2)} = -\mathscr{M}_s^{(2)}, \quad s=0,1,2, \tag{19}$$

$$\mathscr{R}_s^{(1)} = -\left(\mathscr{M}_s^{(1)}+\widetilde{\mathscr{M}}_s^{(1)}\,\mathrm{sgn}(k)\right), \quad s=1,2, \tag{20}$$

$$\mathscr{M}_0^{(n)} = \frac{f_n(1)}{2D(1)}, \qquad \mathscr{M}_s^{(n)} = \frac{f_n(y_s)}{(1-y_s^2)\,D'(y_s)}, \qquad n=0,2 \quad\text{and}\quad s=1,2, \tag{21}$$

$$\mathscr{M}_s^{(1)} = \frac{f_1(y_s)}{D'(y_s)}, \qquad \widetilde{\mathscr{M}}_s^{(1)} = \frac{\tilde{f}_1(y_s)}{D'(y_s)}, \quad s=1,2, \tag{22}$$

while the functions $f_i$ are defined by

$$\begin{aligned} f_0(x) &= \tfrac{1}{2}\left\{8\nu x^4-(-x^2+1)(-2x^2q+1)\right\}\\ &\cdot(n_jn_\ell+m_jm_\ell)\sin^2\theta+\left\{8\nu x^4\sin^2\theta\right.\\ &\left.+(-x^2+1)[-x^2-(-2x^2q+1)\cos^2\theta]\right\}\hat{\beta}_j\hat{\beta}_\ell, \end{aligned} \tag{23}$$

$$f_1(x) = x^3(4\nu-1)(s_j\hat{\beta}_\ell - \hat{\beta}_j s_\ell)\sin\theta, \quad (24)$$

$$\tilde{f}_1(x) = -\tfrac{1}{2}(s_j\hat{\beta}_\ell + \hat{\beta}_j s_\ell)(-2x^2q+1)\sin 2\theta, \quad (25)$$

$$f_2(x) = -\tfrac{1}{2}[8\nu x^4 - (-x^2+1)(-2x^2q+1)] \cdot \left\{ n_j(n_\ell\cos 2\Phi + m_\ell \sin 2\Phi) + m_j(n_\ell \sin 2\Phi - m_\ell \cos 2\Phi)\right\}\sin^2\theta, \quad (26)$$

$$s_j(\Phi) = n_j\cos\Phi + m_j\sin\Phi, \quad (27)$$

and the polynomials $D(x)$ and $D'(x)$ by

$$D(x) = x^4 - 2x^2q + 1 \quad \text{and} \quad D'(x) = -4x^3 + 4xq. \quad (28)$$

Notice that $D'(x)$ is not the derivative of $D(x)$.

A discussion of the properties of the fundamental solution $U_{jl}$ and some aspects of the above expression, together with recommendations for its numerical evaluation can be found in Criado and co-workers (2005, 2008).

### 3.2 Traction fundamental solution

The direct boundary integral equation for surface displacement requires the displacement fundamental solution, and the corresponding traction fundamental solution. The starting point in the evaluation of tractions in an exponentially graded material due to a unit point force is the differentiation of the fundamental solution in displacements $U_{jl}$. These derivatives are used to determine the corresponding strains, and then employing the constitutive law with the tensor of elastic stiffnesses given in (2-3), the corresponding stresses can be obtained.

Differentiation of (4) yields

$$\frac{\partial U_{j\ell}}{\partial x_k}(\boldsymbol{x},\boldsymbol{x}') = \exp\left(-\boldsymbol{\beta}\cdot(\boldsymbol{x}+\boldsymbol{x}')\right) \cdot \left(\frac{\partial U^0_{j\ell}}{\partial x_k}(\boldsymbol{x}-\boldsymbol{x}') + \frac{\partial U^g_{j\ell}}{\partial x_k}(\boldsymbol{x}-\boldsymbol{x}')\right) - \beta_k U_{j\ell}(\boldsymbol{x},\boldsymbol{x}'). \quad (29)$$

Although the derivative of $U^0_{j\ell}$ is strongly singular, this term eventually produces the Kelvin traction kernel for a homogeneous material; the expressions can be found in París and Cañas (1997) and Aliabadi (2002). The derivative of $U^g_{j\ell}$ is weakly singular and can be expressed, in view of (5), as

$$\frac{\partial U^g_{j\ell}}{\partial x_k}(\boldsymbol{x}-\boldsymbol{x}') = -\frac{\delta_{j\ell}}{4\pi\mu_0}\left\{\frac{\mathrm{e}^{-\beta r}(\beta r_{,k})}{r} - \frac{(1-\mathrm{e}^{-\beta r})r_{,k}}{r^2}\right\} + \frac{\partial A_{j\ell}}{\partial x_k}(\boldsymbol{x}-\boldsymbol{x}'), \quad (30)$$

where the derivative of $A_{jl}$ is, according to (7), decomposed into the sum of the derivatives of the integrals $\mathscr{I}_i$

$$\frac{\partial A_{jl}}{\partial x_k}(\boldsymbol{x}-\boldsymbol{x}') = -\frac{\beta}{4\pi(1-\nu)\mu_0}\frac{\partial \mathscr{I}_1}{\partial x_k} - \frac{\beta}{2\pi^2(1-\nu)\mu_0}\left(\frac{\partial \mathscr{I}_2}{\partial x_k} - \frac{\partial \mathscr{I}_3}{\partial x_k} + \frac{\partial \mathscr{I}_4}{\partial x_k} - \frac{\partial \mathscr{I}_5}{\partial x_k}\right). \quad (31)$$

Note that the weakly singular character of $\partial U^g_{j\ell}/\partial x_k$ directly follows from the boundedness of $U^g_{j\ell}$ and the Gauss divergence theorem.

When differentiating $\mathscr{I}_i$ $(i=2,\ldots,5)$, involving double integrals with respect to $\eta$ and $\theta$, it should be taken into account that while their superior limits are constant, their inferior limits are varying with the positions of the field and source points, $\boldsymbol{x}$ and $\boldsymbol{x}'$, as follows:

- Inferior limit of the integral in $\theta$: $\theta_m = \theta_m(\boldsymbol{x},\boldsymbol{x}')$,
- Inferior limit of the integral in $\eta$: $\eta_m = \eta_m(\boldsymbol{x},\boldsymbol{x}',\theta)$.

Thus, derivatives of these double integrals are evaluated by applying the following rule twice:

$$\frac{d}{dx}\int_{A(x)}^{B} f(x,t)\mathrm{d}t = \int_{A(x)}^{B}\frac{\partial f(x,t)}{\partial x}\mathrm{d}t - f(x,A(x))\frac{dA}{dx}. \quad (32)$$

By also taking into account that $\eta_m(\theta=\theta_m) = \pi/2$ and $\Psi_s(\eta=\eta_m)=0$, see Criado (2005), the following expressions are obtained after some al-

gebraic manipulations:

$$\frac{\partial \mathscr{I}_1}{\partial x_k} = \sum_{s=0}^{2}\sum_{n=0}^{2}\int_0^{\pi/2} \mathrm{e}^{-|k|y_s}\sin\theta\left\{\frac{\partial \mathscr{R}_s^{(n)}}{\partial x_k} I_n(Ky_s) + \mathscr{R}_s^{(n)}\left(-y_s\frac{\partial |k|}{\partial x_k} I_n(Ky_s) + \frac{\partial I_n(Ky_s)}{\partial x_k}\right)\right\}\mathrm{d}\theta \tag{33}$$

$$\frac{\partial \mathscr{I}_2}{\partial x_k} = \sum_{s=0}^{2}\int_{\theta_m}^{\pi/2}\sin\theta\left\{\frac{\partial \mathscr{R}_s^{(0)}}{\partial x_k}\int_{\eta_m}^{\pi/2}\sinh\Psi_s\,\mathrm{d}\eta + \mathscr{R}_s^{(0)}\left\{\int_{\eta_m}^{\pi/2}\cosh\Psi_s\frac{\partial \Psi_s}{\partial x_k}\mathrm{d}\eta\right\}\right\}\mathrm{d}\theta \tag{34}$$

$$\frac{\partial \mathscr{I}_3}{\partial x_k} = \sum_{s=0}^{2}\int_{\theta_m}^{\pi/2}\sin\theta\left\{\frac{\partial \mathscr{R}_s^{(2)}}{\partial x_k}\int_{\eta_m}^{\pi/2}\sinh\Psi_s\cos 2\eta\,\mathrm{d}\eta + \mathscr{R}_s^{(2)}\left\{\int_{\eta_m}^{\pi/2}\cosh\Psi_s\cos 2\eta\frac{\partial \Psi_s}{\partial x_k}\mathrm{d}\eta\right\}\right\}\mathrm{d}\theta \tag{35}$$

$$\frac{\partial \mathscr{I}_4}{\partial x_k} = \sum_{s=1}^{2}\int_{\theta_m}^{\pi/2}\sin\theta\left\{\left(\frac{\partial \mathscr{M}_s^{(1)}}{\partial x_k}\right)\int_{\eta_m}^{\pi/2}\cosh\Psi_s\sin\eta\,\mathrm{d}\eta + \mathscr{M}_s^{(1)}\left\{\int_{\eta_m}^{\pi/2}\sinh\Psi_s\sin\eta\frac{\partial \Psi_s}{\partial x_k}\mathrm{d}\eta - \frac{\partial \eta_m}{\partial x_k}\sin\eta_m\right\}\right\}\mathrm{d}\theta \tag{36}$$

$$\frac{\partial \mathscr{I}_5}{\partial x_k} = \sum_{s=1}^{2}\int_{\theta_m}^{\pi/2}\sin\theta\cdot\left\{\left(\frac{\partial \tilde{\mathscr{M}}_s^{(1)}}{\partial x_k}\mathrm{sgn}(k)\right)\int_{\eta_m}^{\pi/2}\sinh\Psi_s\sin\eta\,\mathrm{d}\eta + \tilde{\mathscr{M}}_s^{(1)}\mathrm{sgn}(k)\left\{\int_{\eta_m}^{\pi/2}\cosh\Psi_s\sin\eta\frac{\partial \Psi_s}{\partial x_k}\mathrm{d}\eta\right\}\right\}\mathrm{d}\theta \tag{37}$$

where

$$\frac{\partial \mathscr{R}_s^{(n)}}{\partial x_k} = 0, \quad n=0 \text{ and } n=1 \text{ with } s=0, \tag{38}$$

$$= -\frac{\partial \mathscr{M}_s^{(1)}}{\partial x_k} - \frac{\partial \widetilde{\mathscr{M}}_s^{(1)}}{\partial x_k}\mathrm{sgn}(k), \quad n=1 \text{ with } s=1,2, \tag{39}$$

$$= -\frac{\partial \mathscr{M}_s^{(2)}}{\partial x_k}, \quad n=2, \tag{40}$$

$$\frac{\partial \Psi_s}{\partial x_k} = \frac{\partial K}{\partial x_k}y_s(\sin\eta_m - \sin\eta) + Ky_s\cos\eta_m\frac{\partial \eta_m}{\partial x_k}, \tag{41}$$

$$\frac{\partial I_n}{\partial x_k} = \frac{2}{\pi(-1)^{n/2}}\int_0^{\pi/2}\cos(n\eta)\sinh(Ky_s\sin\eta)\cdot\frac{\partial K}{\partial x_k}y_s\sin\eta\,\mathrm{d}\eta, \quad n=0,2, \tag{42}$$

$$= \frac{2}{\pi}\int_0^{\pi/2}\sin(\eta)\cosh(Ky_s\sin\eta)\frac{\partial K}{\partial x_k}y_s\cdot\sin\eta\,\mathrm{d}\eta, \quad n=1. \tag{43}$$

The derivative of $\eta_m$ is expressed as

$$\frac{\partial \eta_m}{\partial x_k} = \frac{1}{K\cos\eta_m}\left\{\frac{\partial |k|}{\partial x_k} - \sin\eta_m\frac{\partial K}{\partial x_k}\right\}, \tag{44}$$

where

$$\frac{\partial k}{\partial x_k} = \beta\left(\frac{\partial r}{\partial x_k}\cos\theta\cos\Theta + r\cos\theta\frac{\partial\cos\Theta}{\partial x_k}\right), \tag{45}$$

$$\frac{\partial K}{\partial x_k} = \beta\left(\frac{\partial r}{\partial x_k}\sin\theta\sin\Theta + r\sin\theta\frac{\partial\sin\Theta}{\partial x_k}\right). \tag{46}$$

The derivatives of $\mathscr{M}_s^{(n)}$ and $\widetilde{\mathscr{M}}_s^{(n)}$ appearing in

the above expressions are given by:

$$\frac{\partial \mathscr{M}_s^{(n)}}{\partial x_k} = 0, \quad n = 0, \tag{47}$$

$$= \frac{1}{D'(y_s)} \frac{\partial f_1}{\partial x_k}(y_s), \quad n = 1, \tag{48}$$

$$= \frac{1}{D(1)} \frac{\partial f_2}{\partial x_k}(1), \quad n = 2 \text{ with } s = 0, \tag{49}$$

$$= \frac{1}{(1-y_s{}^2) D'(1)} \frac{\partial f_2}{\partial x_k}(1), \quad n = 2 \text{ with } s = 1, 2, \tag{50}$$

$$\frac{\partial \widetilde{\mathscr{M}}_s^{(1)}}{\partial x_k} = \frac{1}{D'(y_s)} \frac{\partial \tilde{f}_1}{\partial x_k}(y_s), \tag{51}$$

where

$$\frac{\partial f_1}{\partial x_k}(x) = x^3(4\nu - 1) \left( \frac{\partial s_j}{\partial x_k} \hat{\beta}_l - \frac{\partial s_l}{\partial x_k} \hat{\beta}_j \right) \sin\theta \tag{52}$$

$$\frac{\partial f_2}{\partial x_k}(x) = -0.5[8\nu x^4 - (-x^2+1)(-2x^2 q+1)] \cdot \left\{ n_j \left( n_l \frac{\partial \cos 2\Phi}{\partial x_k} + m_l \frac{\partial \sin 2\Phi}{\partial x_k} \right) + m_j \left( n_l \frac{\partial \sin 2\Phi}{\partial x_k} - m_l \frac{\partial \cos 2\Phi}{\partial x_k} \right) \right\} \sin^2\theta \tag{53, 54}$$

$$\frac{\partial \tilde{f}_1}{\partial x_k}(x) = -0.5 \left( \frac{\partial s_j}{\partial x_k} \hat{\beta}_l + \frac{\partial s_l}{\partial x_k} \hat{\beta}_j \right) \cdot (-2x^2 q + 1) \sin 2\theta. \tag{55}$$

Finally,

$$\frac{\partial s_j}{\partial x_k} = n_j \frac{\partial \cos\Phi}{\partial x_k} + m_j \frac{\partial \sin\Phi}{\partial x_k} \tag{56}$$

$$\frac{\partial}{\partial x_k} = \frac{\partial}{\partial \tilde{x}_j} \frac{\partial \tilde{x}_j}{\partial x_k} = L_{jk} \frac{\partial}{\partial \tilde{x}_j}, \tag{57}$$

where $L_{1k} = n_k$, $L_{2k} = m_k$, $L_{3k} = \hat{\beta}_k$, and

$$\frac{\partial \cos\Theta}{\partial \tilde{x}_j} = \frac{\delta_{j3}}{r} - \frac{r_3}{r^2} \frac{\partial r}{\partial \tilde{x}_j}, \tag{58}$$

$$\frac{\partial \sin\Theta}{\partial \tilde{x}_j} = \frac{1}{r\sqrt{r^2 - r_3^2}} \left( r \frac{\partial r}{\partial \tilde{x}_j} - r_3 \delta_{j3} \right) - \frac{\sqrt{r^2 - r_3^2}}{r^2} \frac{\partial r}{\partial \tilde{x}_j}, \tag{59}$$

$$\frac{\partial \cos\Phi}{\partial \tilde{x}_j} = \frac{\delta_{j1}}{\sqrt{r^2 - r_3^2}} - \frac{r_1}{(r^2 - r_3^2)^{3/2}} \left( r \frac{\partial r}{\partial \tilde{x}_j} - r_3 \delta_{j3} \right), \tag{60}$$

$$\frac{\partial \sin\Phi}{\partial \tilde{x}_j} = \frac{\delta_{j2}}{\sqrt{r^2 - r_3^2}} - \frac{r_1}{(r^2 - r_3^2)^{3/2}} \left( r \frac{\partial r}{\partial \tilde{x}_j} - r_3 \delta_{j3} \right). \tag{61}$$

Note that the finite integrals in (33-37) can be computed by the standard Gaussian quadrature, except for the integral in (36) where the function $\frac{\partial \eta_m}{\partial x_k}$ appears. This function is weakly singular for $\theta \to \theta_m$ (including a square root singularity) and accurate values of this integral can be achieved, e.g., by the singularity subtraction technique or a special Gauss-Jacobi quadrature. For further details and a comparison of both techniques, which showed that the special quadrature is slightly more accurate, see Criado (2005).

The strains $E_{ij\ell}(\boldsymbol{x}, \boldsymbol{x}')$ associated with the fundamental solution in displacements $U_{j\ell}(\boldsymbol{x}, \boldsymbol{x}')$ are given by

$$E_{ij\ell}(\boldsymbol{x}, \boldsymbol{x}') = \frac{1}{2} \left( \frac{\partial U_{i\ell}}{\partial x_j}(\boldsymbol{x}, \boldsymbol{x}') + \frac{\partial U_{j\ell}}{\partial x_i}(\boldsymbol{x}, \boldsymbol{x}') \right), \tag{62}$$

and incorporating them into the constitutive law defining the elastic stiffnesses (2-3), yields the corresponding stresses

$$\Sigma_{ij\ell} = 2\mu(\boldsymbol{x}) E_{ij\ell}(\boldsymbol{x}, \boldsymbol{x}') + \lambda(\boldsymbol{x}) E_{kk\ell}(\boldsymbol{x}, \boldsymbol{x}') \delta_{ij}. \tag{63}$$

Then, substituting (62) into (63) and using (29)

yields

$$\Sigma_{ij\ell}(\boldsymbol{x}-\boldsymbol{x}') = \exp\left(\boldsymbol{\beta}\cdot(\boldsymbol{x}-\boldsymbol{x}')\right)\left(\Sigma^0_{ij\ell}(\boldsymbol{x}-\boldsymbol{x}')+\Sigma^g_{ij\ell}(\boldsymbol{x}-\boldsymbol{x}')\right), \tag{64}$$

where the strongly singular term $\Sigma^0_{ij\ell}(\boldsymbol{x}-\boldsymbol{x}')$ represents the stress tensor $\sigma_{ij}$ at $\boldsymbol{x}$ originated by a unit point force in direction $\ell$ at $\boldsymbol{x}'$ in the homogeneous elastic isotropic material having Lamé constants $\mu_0$ and $\lambda_0$ (see París and Cañas (1997); Aliabadi (2002)). The weakly singular grading term $\Sigma^g_{ij\ell}(\boldsymbol{x}-\boldsymbol{x}')$ is expressed as:

$$\Sigma^g_{ij\ell}(\boldsymbol{x}-\boldsymbol{x}') = \mu_0\left(\frac{\partial U^g_{i\ell}}{\partial x_j}+\frac{\partial U^g_{j\ell}}{\partial x_i}-\beta_i\left(U^0_{j\ell}+U^g_{j\ell}\right)-\beta_j\left(U^0_{i\ell}+U^g_{i\ell}\right)\right) + \lambda_0\left(\frac{\partial U^g_{k\ell}}{\partial x_k}-\beta_k\left(U^0_{k\ell}+U^g_{k\ell}\right)\right)\delta_{ij}. \tag{65}$$

It is important to notice the differences between the exponential prefactors in the expressions of the kernels $U_{j\ell}$ and $\Sigma_{ij\ell}$ in (4) and (64) and their implications for the behaviour of these kernels.

First, these prefactors imply that while $U_{j\ell}(\boldsymbol{x},\boldsymbol{x}')$ depends on the position of both the source and field points, $\boldsymbol{x}'$ and $\boldsymbol{x}$, $\Sigma_{ij\ell}(\boldsymbol{x}-\boldsymbol{x}')$ depends only on the difference of these points. This difference can be explained by the fact that the equilibrium equation for the displacement fundamental solution $U_{j\ell}$ includes the graded material properties [Martin *et al.* (2002)], whereas the equilibrium equation for the stress fundamental solution $\Sigma_{ij\ell}$:

$$\frac{\partial \Sigma_{ij\ell}}{\partial x_j}+\delta_{i\ell}\delta(\boldsymbol{x}-\boldsymbol{x}')=0, \tag{66}$$

with $\delta(\boldsymbol{x})$ being the three-dimensional Dirac delta, is naturally independent of these material properties.

Second, taking the source point $\boldsymbol{x}'$ fixed (e.g., at the origin of coordinates), the exponential prefactor in (4) diminishes the values of the displacements $U_{j\ell}$ in stiffer zones and increases them in more compliant zones, whereas the exponential prefactor in (64) increases the values of the stresses $\Sigma_{ij\ell}$ in stiffer zones and diminishes them in more compliant zones.

The traction fundamental solution $T_{i\ell}(\boldsymbol{x},\boldsymbol{x}')$, associated with the unit outward normal vector $\mathbf{n}(\boldsymbol{x})$, is obtained from $\Sigma_{ij\ell}(\boldsymbol{x}-\boldsymbol{x}')$ by the Cauchy lemma:

$$T_{i\ell}(\boldsymbol{x},\boldsymbol{x}') = \Sigma_{ij\ell}(\boldsymbol{x}-\boldsymbol{x}')\,n_j(\boldsymbol{x}) \tag{67}$$

$$= \exp\left(\boldsymbol{\beta}\cdot(\boldsymbol{x}-\boldsymbol{x}')\right)\left(T^0_{i\ell}(\boldsymbol{x},\boldsymbol{x}')+T^g_{i\ell}(\boldsymbol{x},\boldsymbol{x}')\right), \tag{68}$$

where, as for the stress, $T^0_{i\ell}(\boldsymbol{x},\boldsymbol{x}')$ represents the well-known strongly singular fundamental solution in tractions for a homogeneous material (with parameters $\mu_0$ and $\lambda_0$) [París and Cañas (1997); Aliabadi (2002)], and $T^g_{i\ell}(\boldsymbol{x},\boldsymbol{x}')$ is the weakly singular grading term obtained from $\Sigma^g_{ij\ell}(\boldsymbol{x}-\boldsymbol{x}')$, $T^g_{i\ell}(\boldsymbol{x},\boldsymbol{x}') = \Sigma^g_{ij\ell}(\boldsymbol{x}-\boldsymbol{x}')\,n_j(\boldsymbol{x})$.

The behaviour of the stresses originated by a unit point force is illustrated in Figure 1, where three-dimensional plots of some components of the stress fundamental solution $\Sigma_{ij\ell}(\boldsymbol{x}-\boldsymbol{x}')$ are shown, the origin of coordinates being coincident with the force application point, i.e. $\boldsymbol{x}'=\mathbf{0}$. All the components presented show some singular behaviour at $\boldsymbol{x}=\mathbf{0}$. Nevertheless, as can be guessed looking at the values and/or variations of the stresses plotted, these singularities are not always of the same kind, which will be explained in the following. The differences between these plots in Figure 1 can be more easily understood if the symmetry and skew-symmetry planes in the corresponding elastic problems for exponentially graded and homogeneous materials are considered.

The stronger singular behaviour of $\Sigma^0_{ij\ell}$ at $\boldsymbol{x}=\mathbf{0}$ in comparison with $\Sigma^g_{ij\ell}$ is dominant in Figures 1 a) and f). Slight differences between behaviour of stresses in these plots can be attributed to the effect of the exponential prefactor, not present in Figure 1 a), and to different contributions due to $\Sigma^g_{ij\ell}$.

The components $\Sigma^0_{ij\ell}$ corresponding to plots in Figures 1 b) to e) vanish (which can be shown by applying standard symmetry arguments), hence the stress values shown in these plots are exclu-

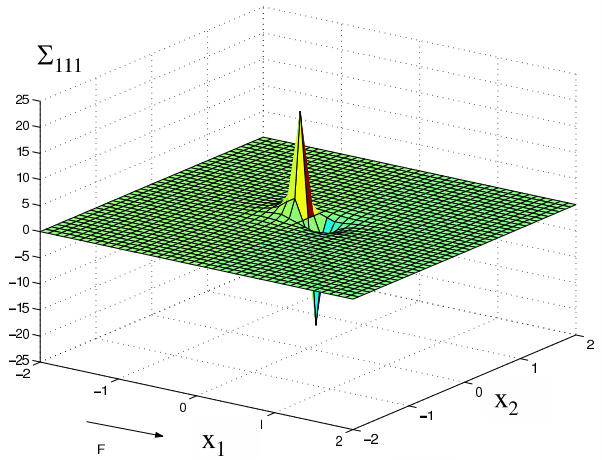


(a) $\Sigma_{111}(x_1,x_2,0)$

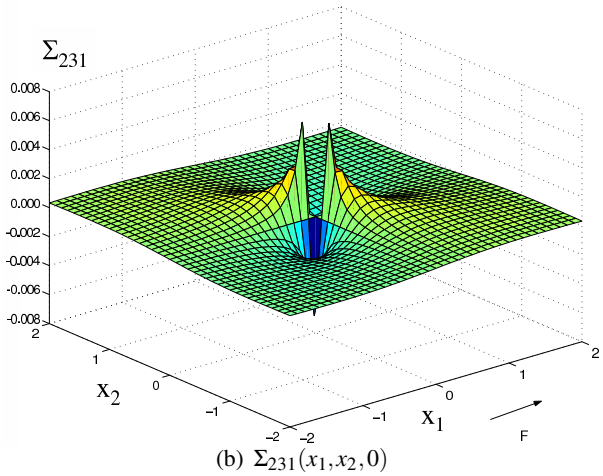


(b) $\Sigma_{231}(x_1,x_2,0)$

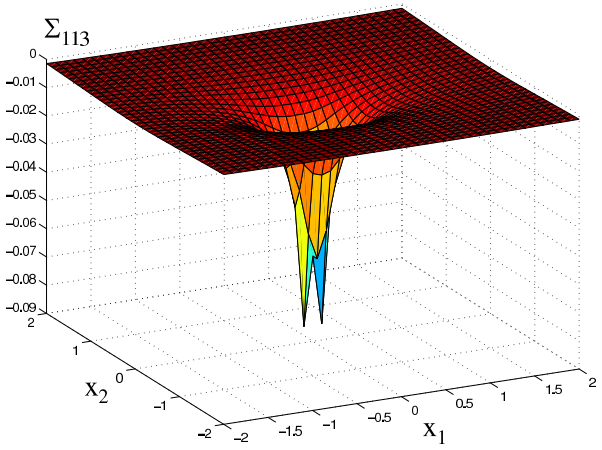


(c) $\Sigma_{113}(x_1,x_2,0)$

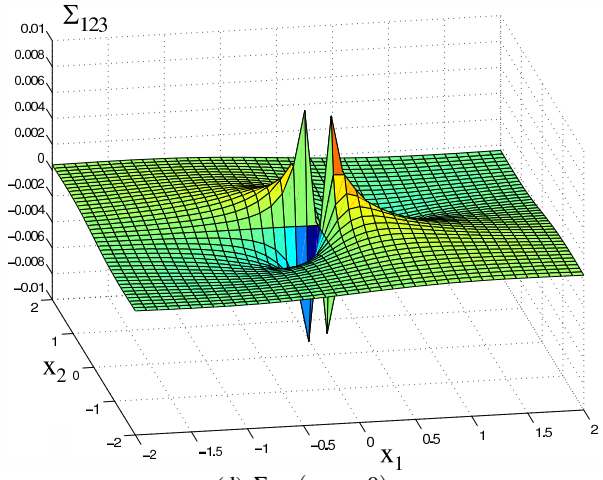


(d) $\Sigma_{123}(x_1,x_2,0)$

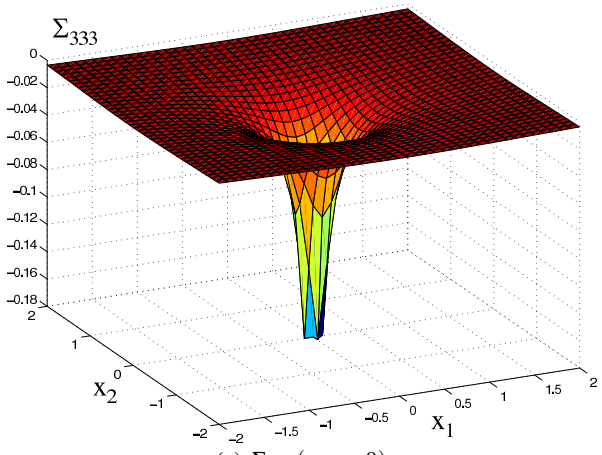


(e) $\Sigma_{333}(x_1,x_2,0)$

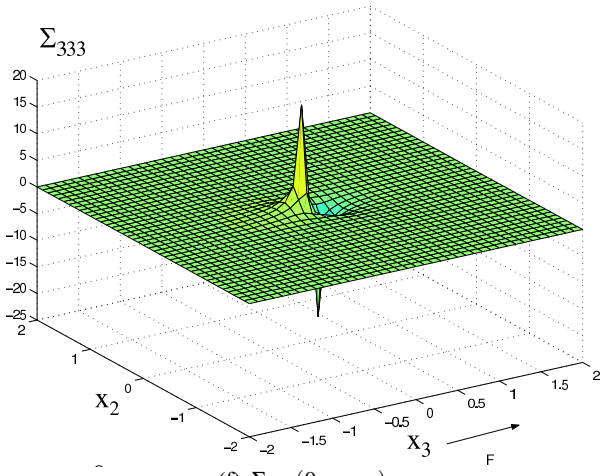


(f) $\Sigma_{333}(0,x_2,x_3)$

Figure 1: Components of the $\Sigma_{ijk}$ kernel for $\mu_0 = 4$, $\nu = 0.35$ and grading parameter $\boldsymbol{\beta} = (0,0,0.1)$.

sively given by the components of $\Sigma^g_{ij\ell}$ times the exponential prefactor.

Finally, in order to show in a very clear way the differences between the stress fundamental solutions in homogeneous and exponentially graded materials, components $\Sigma_{333}(0,0,x_3)$ and $\Sigma^0_{333}(0,0,x_3)$ are plotted in Figure 2. It can be seen how the skew-symmetric character of stresses in the homogeneous material is changed in presence of a grading, in agreement with the above explained effect of the exponential prefactor.

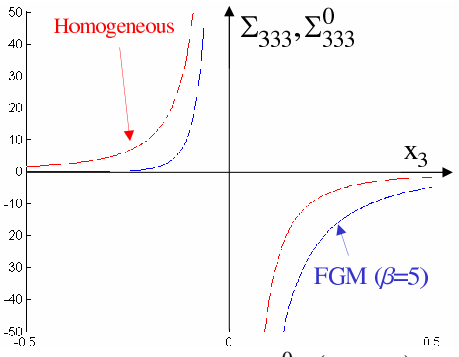


Figure 2: Component $\Sigma^0_{333}(0,0,x_3)$ (corresponding to the homogeneous material) and $\Sigma_{333}(0,0,x_3)$ for $\mu_0 = 4$, $\nu = 0.35$ and grading parameter $\boldsymbol{\beta} = (0,0,5)$.

## 4 Boundary Element Method

The boundary integral formulation for an isotropic, exponentially graded body $\Omega \subset \mathbb{R}^3$ with a bounded (Lipschitz and piecewise smooth) boundary $\partial\Omega = \Gamma$ will be briefly discussed in this section. The derivation follows the standard procedures for a homogeneous material [París and Cañas (1997); Aliabadi (2002)]. Starting from the 2nd Betti Theorem of reciprocity of work for a graded material, one can derive the corresponding Somigliana identity:

$$C_{i\ell}(\boldsymbol{x}')u_i(\boldsymbol{x}') + \int\!\!\!\!\!\!-_{\Gamma} T_{i\ell}(\boldsymbol{x},\boldsymbol{x}')u_i(\boldsymbol{x})dS(\boldsymbol{x}) = \int_{\Gamma} U_{i\ell}(\boldsymbol{x},\boldsymbol{x}')t_i(\boldsymbol{x})dS(\boldsymbol{x}), \quad (69)$$

expressing the displacements $u_i(\boldsymbol{x}')$ at a domain or boundary point $\boldsymbol{x}' \in \Omega \cup \Gamma$ in terms of the boundary displacements $u_i(\boldsymbol{x})$ and tractions $t_i(\boldsymbol{x})$, $\boldsymbol{x} \in \Gamma$. Notice that zero body forces have been considered in (69). The strongly singular traction kernel integral is evaluated in the Cauchy principal value sense, and

$$C_{i\ell}(\boldsymbol{x}') = \lim_{\varepsilon \to 0_+} \int_{S_\varepsilon(\boldsymbol{x}')\cap\Omega} T_{i\ell}(\boldsymbol{x},\boldsymbol{x}')dS(\boldsymbol{x}) \quad (70)$$

is the coefficient tensor of the free term, $S_\varepsilon(\boldsymbol{x}')$ being a spherical surface of radius $\varepsilon$ centered at $\boldsymbol{x}'$ and oriented by the unit normal vectors pointing to the center. It is important to note that, despite the complexity of the $T_{i\ell}$ kernel expression, this evaluation is not a problem. The weakly singular grading term and the exponential prefactor in (68) will play no role in the limit procedure in (70). Thus, the value of $C_{i\ell}$ in (70) coincides with the value of $C_{i\ell}$ for the homogeneous isotropic material whose properties are defined by the Lamé constants $\lambda_0$ and $\mu_0$, *i.e.*,

$$C_{i\ell}(\boldsymbol{x}') = \lim_{\varepsilon \to 0_+} \int_{S_\varepsilon(\boldsymbol{x}')\cap\Omega} T^0_{i\ell}(\boldsymbol{x},\boldsymbol{x}')dS(\boldsymbol{x}). \quad (71)$$

Hence, $C_{i\ell}(\boldsymbol{x}') = \delta_{i\ell}$ for $\boldsymbol{x}' \in \Omega$, $C_{i\ell}(\boldsymbol{x}') = \frac{1}{2}\delta_{i\ell}$ for $\boldsymbol{x}' \in \Gamma$ situated at a smooth part of $\Gamma$, and for an edge or corner point of $\Gamma$, $C_{i\ell}(\boldsymbol{x}')$ is given by the size, shape and spatial orientation of the interior solid angle at $\boldsymbol{x}'$. A general explicit expression of the symmetric tensor $C_{i\ell}(\boldsymbol{x}')$ in terms of the unit vectors tangential to the boundary edges and the unit outward normal vectors to the boundary surfaces at $\boldsymbol{x}'$ can be found in Mantič (1993).

For an unbounded domain $\Omega$, the form of the Somigliana identity in (69) holds if the following radiation condition [Costabel and Dauge (1997)] for the displacement solution $u_i$ and the corresponding traction solution $t_i$ is fulfilled for any fixed $\boldsymbol{x}' \in \Omega$:

$$\lim_{\rho\to\infty} \int_{\Gamma_\rho} \left( U_{i\ell}(\boldsymbol{x},\boldsymbol{x}')t_i(\boldsymbol{x}) - T_{i\ell}(\boldsymbol{x},\boldsymbol{x}')u_i(\boldsymbol{x}) \right) dS(\boldsymbol{x}) = 0, \quad (72)$$

where $\Gamma_\rho$ is the spherical surface of radius $\rho$ centered at the origin of coordinates. In fact, (72) implies that the integral in (72) vanishes for any sufficiently large $\Gamma_\rho$ including $\Gamma$ in its interior and

any $\boldsymbol{x}' \in \Omega$, $\|\boldsymbol{x}'\| < \rho$. A further study of (72) using a detailed knowledge of the behaviour of $U^g_{jl}(\boldsymbol{x}-\boldsymbol{x}')$ for $r \to \infty$ (apparently not available at present due to the cumbersome expression of $A_{jl}$ given in (7)) might be necessary in the deduction of a more explicit and equivalent expression of this radiation condition in the classical form (see Costabel and Dauge (1997) for some standard examples). This classical form of (72) would be very useful for practical applications of (69) to infinite domains.

The numerical implementation of (69) in this work employs standard approximation techniques. A collocation approximation based upon a nine-node continuous quadrilateral quadratic isoparametric element is employed to interpolate the boundary and the boundary functions. The evaluation of regular integrals is accomplished by Gaussian quadrature with $8 \times 8$ integration points, whereas an adaptive element subdivision following the procedure developed in Lachat and Watson (1976) is utilized for nearly singular integrals. A standard triangle to square transformation [Lachat and Watson (1976)] is employed to handle the weakly singular integrals involving the kernel $U_{i\ell}$, and the rigid body motion procedure is invoked for evaluating the sum of the coefficient tensor of the free term $C_{i\ell}$ and the Cauchy principal value integral with the kernel $T_{i\ell}$.

## 5 Numerical Results

The expression for the $T_{i\ell}(\boldsymbol{x},\boldsymbol{x}')$ kernel is clearly quite complicated, and thus it is necessary to verify that these formulas and their numerical implementation are correct. This is accomplished in this section using two relatively simple problems having known exact solutions.

Consider the cube $\Omega = (0,\ell)^3$ wherein the material is exponentially graded in the $x_3$-direction. The grading coefficient $\beta$ in the numerical tests will be chosen as $(\ln 2)/\ell$ or $(\ln 7)/\ell$; thus, the Young modulus increases in the $x_3$-direction 4 or 49 times, respectively, *i.e.*, $E(x_3=\ell)/E_0 = 4$ or 49, where $E_0 = E(x_3 = 0)$. In both test problems, symmetry boundary conditions are imposed on the three faces coincident with the coordinate planes: $x_1 = 0$, $x_2 = 0$ and $x_3 = 0$. Elastic solutions in this cube having different loads and different Poisson ratios $\nu$ will be studied using three very coarse meshes, denoted as $A$, $B$ and $C$. Mesh $A$ has one element per face, and therefore a total of 6 elements, while the meshes $B$ and $C$ are obtained by dividing each element of mesh $A$ parallel to the $x_3$-direction into 2 and 3 uniform elements, respectively. This results in a total of 10 and 14 elements. These meshes are shown in Figure 3, together with the above symmetry boundary conditions.

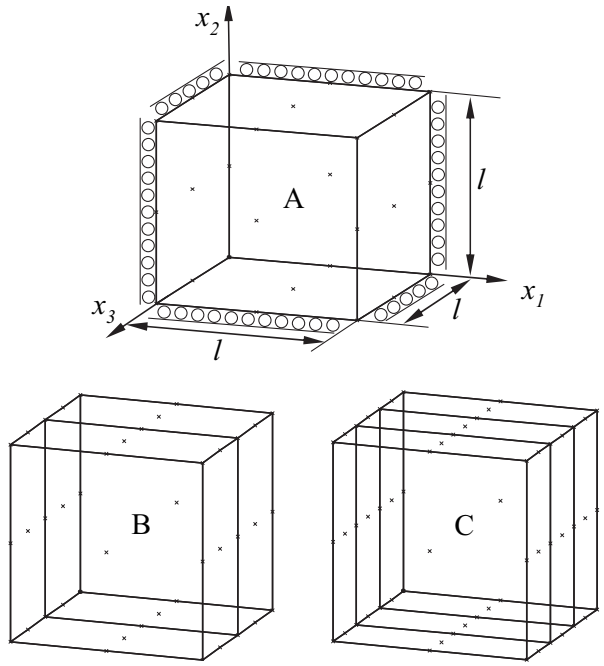


Figure 3: Three BEM discretizations of cube ($A$, $B$ and $C$) using 6, 10 and 14 elements, respectively.

The percentages of the normalized error in stresses and displacements will be computed as

$$\begin{aligned} \%Err(\sigma_{ij}) &= \frac{\sigma_{ij}^{\text{BEM}} - \sigma_{ij}^{\text{anal.}}}{\sigma_0} \times 100, \\ \%Err(u_i) &= \frac{u_i^{\text{BEM}} - u_i^{\text{anal.}}}{\max\, u_i^{\text{anal.}}} \times 100, \end{aligned} \tag{73}$$

where $\sigma_0$ is a nominal stress involved in the definition of each problem.

Table 1: Normalized errors in $\sigma_{33}$ at the plane $x_3 = 0$. Grading coefficient $\beta = (\ln 2)/\ell$. Meshes $A$, $B$ and $C$.

| | | Normalized error (%) | | |
|---|---|---|---|---|
| Node | Coordinates | $A$ | $B$ | $C$ |
| 1 | (0, 0, 0) | -0.9931 | -0.2070 | 0.0149 |
| 2 | (0.5$\ell$, 0, 0) | 0.0311 | -0.0080 | 0.0123 |
| 3 | ($\ell$, 0, 0) | -0.4273 | -0.1961 | -0.1951 |
| 4 | (0, 0.5$\ell$, 0) | 0.0311 | -0.0078 | 0.0128 |
| 5 | (0.5$\ell$, 0.5$\ell$, 0) | 1.0948 | 0.1920 | -0.0544 |
| 6 | ($\ell$, 0.5$\ell$, 0) | 0.3084 | -0.0583 | 0.0260 |
| 7 | (0, $\ell$, 0) | -0.4276 | -0.1967 | -0.1966 |
| 8 | (0.5$\ell$, $\ell$, 0) | 0.3085 | -0.0581 | 0.0266 |
| 9 | ($\ell$, $\ell$, 0) | 0.2416 | -0.1283 | -0.368 |

Table 2: Normalized errors in $u_3$ along the edge $x_1 = x_2 = \ell$. Grading coefficient $\beta = (\ln 2)/\ell$. Meshes $A$, $B$ and $C$.

| | | Normalized error (%) | | |
|---|---|---|---|---|
| Node | Coordinates | $A$ | $B$ | $C$ |
| 1 | ($\ell$, $\ell$, 0.17$\ell$) | | | 0.0010 |
| 2 | ($\ell$, $\ell$, 0.25$\ell$) | | -0.0245 | |
| 3 | ($\ell$, $\ell$, 0.33$\ell$) | | | 0.0000 |
| 4 | ($\ell$, $\ell$, 0.50$\ell$) | -0.2638 | -0.0335 | -0.0006 |
| 5 | ($\ell$, $\ell$, 0.67$\ell$) | | | -0.0015 |
| 6 | ($\ell$, $\ell$, 0.75$\ell$) | | -0.0411 | |
| 7 | ($\ell$, $\ell$, 0.83$\ell$) | | | -0.0029 |
| 8 | ($\ell$, $\ell$, $\ell$) | -0.3913 | -0.0383 | -0.0031 |

Table 3: Normalized errors in $\sigma_{33}$ at the plane $x_3 = 0$. Grading coefficient $\beta = (\ln 7)/\ell$. Mesh $B$.

| | | Normalized error (%) |
|---|---|---|
| Node | Coordinates | $B$ |
| 1 | (0, 0, 0) | 0.0145 |
| 2 | (0.5$\ell$, 0, 0) | 0.8022 |
| 3 | ($\ell$, 0, 0) | -0.4717 |
| 4 | (0, 0.5$\ell$, 0) | 0.8924 |
| 5 | (0.5$\ell$, 0.5$\ell$, 0) | 0.1422 |
| 6 | ($\ell$, 0.5$\ell$, 0) | 0.8024 |
| 7 | (0, $\ell$, 0) | 0.6548 |
| 8 | (0.5$\ell$, $\ell$, 0) | 0.8927 |
| 9 | ($\ell$, $\ell$, 0) | 0.0140 |

### *5.1 Example 1*

Let the cube $\Omega$, with the Poisson ratio $\nu = 0.0$, be subjected to a constant normal traction $\sigma_0$ on its face $x_3 = \ell$ (*i.e.* $\sigma_{33}(x_1, x_2, \ell) = \sigma_0$), the other faces, $x_1 = \ell$ and $x_2 = \ell$, being traction free.

The exact solution of this problem can be found in Criado *et al.* (2008): $u_3(\boldsymbol{x}) = (1 - \exp(-2\beta x_3))\sigma_0/2\beta E_0$, $u_1 = u_2 = 0$, $\sigma_{33}(\boldsymbol{x}) = \sigma_0$ and the remaining stresses vanishing, $\sigma_{ij} = 0$ for $(i, j) \neq (3, 3)$.

The accuracy of the solution when refining the mesh can be observed in Tables 1 and 2 where the percentage of the normalized error in the normal stress $\sigma_{33}(x_1, x_2, 0)$ and the displacement $u_3(\ell, \ell, x_3)$ are presented for the smaller value of the grading coefficient ($\beta = (\ln 2)/\ell$). Although the convergence is not uniform, due to the very coarse meshes used, the level of the errors is excellent. In particular, for the extremely coarse mesh $A$ the maximum error in stresses is already about 1%, whereas mesh $C$ provides errors less than 0.2%. Errors in displacements are even smaller, less than 0.4% for mesh $A$ and less than 0.004% for mesh $C$.

The results obtained for the substantially stronger grading ($\beta = (\ln 7)/\ell$) are shown in Tables 3 and 4. Although, as could be expected, the level of error is somewhat higher than in the previous case, errors in stresses and displacements, respectively, under 0.9% and 0.5% are still excellent in view of the relatively coarse mesh $B$ used.

### *5.2 Example 2*

In this example, let the cube $\Omega$ be subjected to a constant normal displacement $\sigma_0\ell/E_0$ on its face $x_1 = \ell$ (*i.e.* $u_1(\ell, x_2, x_3) = \sigma_0\ell/E_0$), the other faces, $x_2 = \ell$ and $x_3 = \ell$, being traction free. In addition, the Poisson ratio is specified as $\nu = 0.3$ and the grading coefficient $\beta = (\ln 2)/\ell$.

The exact solution of this problem can also be found in Criado *et al.* (2008): $u_1(\boldsymbol{x}) = \sigma_0 x_1/E_0$, $u_2 = -\nu\sigma_0 x_2/E_0$, $u_3 = -\nu\sigma_0 x_3/E_0$, $\sigma_{11}(\boldsymbol{x}) = \sigma_0 \exp(2\beta x_3)$, with the remaining stresses vanishing, $\sigma_{ij} = 0$ for $(i, j) \neq (1, 1)$.

Tables 5, 6 and 7 present the normalized errors obtained. As in the previous example, an excel-

Table 4: Normalized errors in $u_3$ along the edge $x_1 = x_2 = \ell$. Grading coefficient $\beta = (\ln 7)/\ell$. Mesh $B$.

| | | Normalized error (%) |
|---|---|---|
| Node | Coordinates | $B$ |
| 1 | $(\ell, \ell, 0.25)$ | 0.2521 |
| 2 | $(\ell, \ell, 0.5\ell)$ | 0.4067 |
| 3 | $(\ell, \ell, 0.75\ell)$ | 0.4452 |
| 4 | $(\ell, \ell, \ell)$ | 0.4462 |

Table 5: Normalized errors in $\sigma_{11}$ along the edge $x_1 = x_2 = 0$. Grading coefficient $\beta = (\ln 2)/\ell$. Meshes $A$, $B$ and $C$.

| | | Normalized error (%) | | |
|---|---|---|---|---|
| Node | Coordinates | $A$ | $B$ | $C$ |
| 1 | (0, 0, 0) | 0.713307 | 0.090730 | 0.019430 |
| 2 | $(0, 0, 0.17\ell)$ | | | -0.035429 |
| 3 | $(0, 0, 0.25\ell)$ | | -0.005309 | |
| 4 | $(0, 0, 0.33\ell)$ | | | 0.009429 |
| 5 | $(0, 0, 0.50\ell)$ | 0.023527 | 0.023982 | -0.065233 |
| 6 | $(0, 0, 0.67\ell)$ | | | -0.000443 |
| 7 | $(0, 0, 0.75\ell)$ | | -0.001453 | |
| 8 | $(0, 0, 0.83\ell)$ | | | -0.105120 |
| 9 | $(0, 0, \ell)$ | -1.093050 | -0.203555 | -0.085220 |

Table 6: Normalized errors in $u_1$ along the line $x_2 = 0.5\ell$ and $x_3 = \ell$. Grading coefficient $\beta = (\ln 2)/\ell$. Meshes $A$, $B$ and $C$.

| | | Normalized error (%) | | |
|---|---|---|---|---|
| Node | Coordinates | $A$ | $B$ | $C$ |
| 1 | $(0.5\ell, 0.5\ell, \ell)$ | 0.0639 | 0.0023 | -0.0564 |
| 2 | $(\ell, 0.5\ell, \ell)$ | 0.1677 | 0.0215 | -0.0287 |

Table 7: Normalized errors in $u_3$ along the line $x_1 = \ell$ and $x_2 = 0.5\ell$. Grading coefficient $\beta = (\ln 2)/\ell$. Meshes $A$, $B$ and $C$.

| | | Normalized error (%) | | |
|---|---|---|---|---|
| Node | Coordinates | $A$ | $B$ | $C$ |
| 1 | $(\ell, 0.5\ell, 0.17\ell)$ | | | 0.0004 |
| 2 | $(\ell, 0.5\ell, 0.25\ell)$ | | -0.0036 | |
| 3 | $(\ell, 0.5\ell, 0.33\ell)$ | | | 0.0018 |
| 4 | $(\ell, 0.5\ell, 0.50\ell)$ | -0.0567 | -0.0067 | 0.0076 |
| 5 | $(\ell, 0.5\ell, 0.67\ell)$ | | | 0.0161 |
| 6 | $(\ell, 0.5\ell, 0.75\ell)$ | | -0.0063 | |
| 7 | $(\ell, 0.5\ell, 0.83\ell)$ | | | 0.0207 |
| 8 | $(\ell, 0.5\ell, \ell)$ | -0.0642 | -0.0117 | 0.0147 |

lent accuracy has been obtained, although the results do not show a uniform convergence, again due to the very coarse meshes used. Specifically, the errors in the normal stress $\sigma_{11}(0,0,x_3)$ are less than 1.1% for mesh $A$ and 0.11% for mesh $C$, errors in the displacement $u_1(x_1, 0.5\ell, \ell)$ are less than 0.17% for mesh $A$ and 0.06% for mesh $C$, and errors in displacement $u_3(\ell, 0.5\ell, x_3)$ are less than 0.07% for mesh $A$ and 0.021% for mesh $C$.

## 6 Conclusions

The numerical solution of the 3D Somigliana displacement identity for isotropic elastic exponentially graded materials by a direct collocation BEM code has been successfully developed.

First, a new expression of the strongly singular fundamental solution in tractions, $T_{j\ell}$, for such materials has been deduced. Then, the fundamental solutions in displacements, $U_{j\ell}$, and tractions, $T_{j\ell}$, have been implemented in the BEM code. To the best knowledge of the authors, this is the first implementation of a 3D direct BEM code for such materials. The numerical solution of a few examples with known analytic solutions have produced excellent accuracy, confirming the correctness of the kernel functions and their implementation.

The remaining problem to use this approach in a convenient way for real size problems from now on is simply computation time: the evaluation of the Green's function kernels for exponentially graded materials is quite expensive and techniques to reduce this cost, which is at present substantially higher than for homogeneous materials (about 90 times higher CPU time for some small problems), must be developed. One option is to develop faster techniques for computing the kernels, perhaps by means of suitable approximations of $U_{j\ell}$ and $T_{j\ell}$, and another is to implement the BEM code on a multi-processor machine. This last option can be carried out using a domain decomposition method, this approach currently in progress by the authors for the solution of some medium-scale problems.

**Acknowledgement:** The present work has been developed during the stay of R. Criado at the Oak

Ridge National Laboratory (funded by the Applied Mathematical Sciences Research Program of the Office of Mathematical, Information, and Computational Sciences, U.S. Department of Energy, under contract DE-AC05-00OR22725 with UT-Battelle), and the stays of J.E. Ortiz and L. Gray at the University of Seville (funded by the Spanish Ministry of Education, Culture and Sport; Juan de la Cierva Programm and SAB2003-0088, respectively). V. Mantič and F. París have been supported by the Spanish Ministry of Science and Technology through project MAT2003-03315.

## References

**Aliabadi, M.H.** (2002): *The Boundary Element Method, Volume 2 Applications in Solids and Structures.* John Wiley & Sons, Chichester.

**Anlas, G.; Santare, M.H.; Lambros, J.** (2000): Numerical calculation of stress intensity factors in functionally graded materials. *International Journal of Fracture*, vol. 104, pp. 131–143.

**Atluri, S.N.; Shen, S.** (2002): The meshless local Petrov-Galerkin (MLPG) method: A simple & less costly alternative to the finite element and boundary element method. *CMES: Computer Modeling in Engineering & Sciences*, vol. 3, pp. 11–52.

**Berger, J.R.; Martin, P.A.; Mantič, V.; Gray, L.J.** (2005): Fundamental solution for steady-state heat transfer in an exponentially graded anisotropic material. *ZAMP*, vol. 56, pp. 293–303.

**Chan, Y.; Gray, L.J.; Kaplan, T.; Paulino, G.H.** (2004): Green's function for a two-dimensional exponentially graded elastic medium. *Proceedings Royal Society London A*, vol. 460, pp. 1689–1706.

**Ching, H.K.; Chen, J.K.** (2006): Thermomechanical analysis of functionally graded composites under laser heating by the MLPG method. *CMES: Computer Modeling in Engineering & Sciences*, vol. 13, pp. 199–218.

**Clements, D.L.** (1998): Fundamental solutions for second order linear elliptic partial differential equations. *Computational Mecahnics*, vol. 22, pp. 26–31.

**Clements, D.L.; Budhi, W.S.** (1999): A boundary element method of the solution of a class of steady-state problems for anisotropic media. *Journal of Heat Transfer*, vol. 121, pp. 462–465.

**Costabel, M.; Dauge, M.** (1997): On representation formulas and radiation conditions. *Mathematical Methods in the Applied Sciences*, vol. 20, pp. 133–150.

**Criado, R.** (2005): *Desarrollo y programación de la solución fundamental en desplazamientos y tensiones para el problema elástico tridimensional en materiales exponencialmente graduados isótropos*. Proyecto Fin de Carrera, ETSI, Universidad de Sevilla.

**Criado, R.; Gray, L.J.; Mantič, V.; París, F.** (2008): Green's function evaluation for three dimensional exponentially graded elasticity. *International Journal for Numerical Methods in Engineering* (in press).

**Gray, L.J.; Kaplan, T; Richardson, J.D.; Paulino, G.H.** (2003): Green's function and boundary integral analysis for exponentially graded materials: heat conduction. *Journal of Applied Mechanics*, vol. 40, pp. 543–549.

**Han, F.; Pan, E.; Roy, A.K.; Yue, Z.Q.** (2006): Responses of piezoelectric, transversely isotropic, functionally graded, and multilayered half spaces to uniform circular surface loadings. *CMES: Computer Modeling in Engineering & Sciences*, vol. 14, pp. 15–30.

**Kim, J.; Paulino, G.H.** (2002a): Finite element evaluation of mixed mode stress intensity factors in functionally graded materials. *International Journal for Numerical Methods in Engineering*, vol. 53, pp. 1903–1935.

**Kim, J.; Paulino, G.H.** (2002b): Isoparametric graded finite elements for nonhomogeneous isotropic and orthotropic materials. *Journal of Applied Mechanics*, vol. 69, pp. 502–514.

**Kuo, H.Y.; Chen, T.** (2005): Steady and transient Greens functions for anisotropic conduction in an exponentially graded solid. *International Journal of Solids and Structures*, vol. 42, pp. 1111–1128.

**Lachat, J.C.; Watson, J.O.** (1976): Effective numerical treatment of boundary integral equations: a formulation for three-dimensional elastostatics. *International Journal for Numerical Methods in Engineering*, vol.10, pp. 991–1005.

**Lee, Y.-D.; Erdogan, F.** (1998): Interface cracking of FGM coatings under steady-state heat flow. *Engineering Fracture Mechanics*, vol. 59, pp. 361–380.

**Mantič, V.** (1993): A new formula for the C-matrix in the Somigliana identity. *Journal of Elasticity*, vol. 33, pp. 191–201.

**Martin, P.A.; Richardson, J.D.; Gray, L.J.; Berger, J.R.** (2002): On Green's function for a three-dimensional exponentially graded elastic solid. *Proceedings Royal Society London A*, vol. 458, pp. 1931–1947.

**Núñez, J.P.; Mantič, V.; París, F.; Berger, J.** (2002): Boundary element analysis of heat transfer at an interface crack in an FGM coating. In *ECCM-10, Composites for the Future, 10th European Conference on Composite Materials (CD)*, The European Society for Composite Materials (ESCM), Brugge.

**París, F.; Cañas, J.** (1997): *Boundary Element Method, Fundamentals and Applications.* Oxford University Press, Oxford.

**Paulino, G.H.; Kim, J.** (2004): A new approach to compute T-stress in functionally graded materials by means of the interaction integral method. *Engineering Fracture Mechanics*, vol. 71, pp. 1907–1950.

**Paulino, G.H.; Sutradhar, A.; Gray, L.J.** (2002): Boundary element methods for functionally graded materials. In S.A. Kinnas (Ed.) *IABEM 2002 (CD)*, The University of Texas at Austin.

**Santare, M.H.; Lambros, J.** (2000): Use of graded finite elements to model the behavior of nonhomogeneous materials. *Journal of Applied Mechanics*, vol. 67, pp. 819–822.

**Seyrafian, S.; Gatmiri, B.; Noorzad, A.** (2006): Green functions for a continuously nonhomogeneous saturated media. *CMES: Computer Modeling in Engineering & Sciences*, vol. 15, pp. 115–126.

**Shaw, R.P.; Makris, N.** (1992): Green's function for Helmholtz and Laplace equations in heterogeneous media. *Engineering Analysis with Boundary Elements*, vol. 10, pp. 179–183.

**Sládek, J.; Sládek, V.; Kriváček, J.; Zhang, Ch.** (2005): Meshless local Petrov-Galerkin method for stress and crack analysis in 3-D axisymmetric FGM bodies. *CMES: Computer Modeling in Engineering & Sciences*, vol. 8, pp. 259–270.

**Sládek, J.; Sládek, V.; Zhang, Ch.** (2004): Application of meshless local Petrov-Galerkin (MLPG) method to elastodynamic problems in continuously nonhomogeneous solids. *CMES: Computer Modeling in Engineering & Sciences*, vol. 4, pp. 637–648.

**Sládek, J.; Sládek, V.; Zhang, Ch., Solek, P.; Starek, L.** (2007): Fracture analyses in continuously nonhomogeneous piezoelectric solids by the MLPG. *CMES: Computer Modeling in Engineering & Sciences*, vol. 19, pp. 247–262.

**Sutradhar, A.; Paulino, G. H.** (2004): The simple boundary element method for transient heat conduction in functionally graded materials. *Computer Methods in Applied Mechanics and Engineering*, vol. 193, pp. 4511–4539.

**Suresh, S.; Mortensen A.** (1998): *Fundamentals of Functionally Graded Materials.* IOM Communications, London.